Research Square

Preprints are preliminary reports that have not undergone peer review.
They should not be considered conclusive, used to inform clinical practice,
or referenced by the media as validated information.

Direct Shot Velocity Measurement and a Numerical Simulation of Shot Peening for Welded Joints

Koji Kinoshita

kinoshita@fukuoka-u.ac.jp

Fukuoka University Faculty of Engineering

Yukina Takai

JFE Engineering

Yuki Ono

Aalto University School of Engineering: Aalto-yliopisto Insinooritieteiden korkeakoulu

Yuki Banno

Gifu University Faculty of Engineering Graduate School of Engineering: Gifu Daigaku Kogakubu Daigakuin Kogaku Kenkyuka

Kazuma Inoue

Japan Construction Method and Machinery Research Institute

Research Article

Keywords: FEM, Shot peening, Ultra high-speed camera, Residual stress distribution

Posted Date: November 5th, 2025

DOI: https://doi.org/10.21203/rs.3.rs-7895821/v1

License: This work is licensed under a Creative Commons Attribution 4.0 International License.
Read Full License

INTERNATIONAL INSTITUTE OF WELDING
A world of joining experience

JAPANESE DELEGATION

XIII-3000-2023

Direct Shot Velocity Measurement and a Numerical Simulation of Shot Peening for Welded Joints

Koji Kinoshita*, Yukina Takai, Yuki Ono, Yuki Banno, Kazuma Inoue
Fukuoka University (Fukuoka, Japan, Corresponding author: kinoshita@fukuoka-u.ac.jp)
JFE Engineering (Tokyo, Japan, takai-yukina@jfe-eng.co.jp)
Aalto University (Helsinki, Finland, yuki.ono@aalto.fi)
Gifu University (Gifu, Japan, yuki.banno.m6@f.gifu-u.ac.jp)
Japan Construction Method and Machinery Research Institute (Shizuoka, Japan, inoue_k@cmi.or.jp)

Abstract

This study experimentally performed direct measurements of shot velocity using an ultra-high-speed camera. Two nozzle types and distance between nozzle and specimen were prepared, and shot velocity was measured from shot movement captured by image processing. Measured shot velocity agrees well with a value generally reported in previous studies, despite the shot velocity increases with increasing the distance between the nozzle and the specimen in case of a straight nozzle. Then, a numerical simulation on shot peening was conducted using RADIOSS, reflecting the shot velocity measurement results. The simulated residual stress was compared with measurement results obtained on base materials near weld toes. As a result, the shot peening analysis successfully captured the depths associated with the minimum compressive residual stress and the plastic region. Based on this analysis model, this study investigated the influence of shot angle, friction, and material hardening rules on the residual stress distribution. The investigation results showed that the shot angle and friction might be key influencing factors for better estimating the amount of compressive residual stress. Thus, the shot peening angle to weld toes should be certainly controlled.

Keywords: FEM, Shot peening, Ultra high-speed camera, Residual stress distribution

1. Introduction

Steel bridges generally experience a number of changes in applied live loads from traffic, and

fatigue cracks continue to be reported particularly for welded joints [1]. Thus, there is a significant need for enhancing the fatigue strength of welded joints in existing steel bridges. An practical approach to this need is utilizing post-weld treatment methods. Among these methods, shot peening technique has been used globally in many industries such as automobiles and aircrafts, known for its ability to induce beneficial compressive residual stress in wide surfaces of steel components through the impact of numberless shots. Previously, shot peening has also proven effective in enhancing the fatigue strength of welded joints by introducing compressive residual stress to the critical weld toes [2-4]. Despite this potential benefit, the application of shot peening in existing steel bridges remains limited due to the challenge of managing shot media on bridge sites; one attempt exists in 1991 [5]. To address this, shot peening for existing steel bridges has been developed, employing a novel vacuuming technique that enables collection and reuse of shot media at bridge sites and utilization of the same facility as conventional blast technique for repainting [6-8]. The implementation of this shot peening has been investigated through residual stress measurements on both actual existing bridges and welded joint specimens, as well as fatigue testing for the specimens at stress ratio R = -1 [6-8] As a result, the previous studies [7-8] have demonstrated a stable introduction of compressive residual stress in existing bridges. Furthermore, these studies established the treatment conditions and quality control method based on surface coverage and arc height for fatigue strength improvement for welded joints. Depending on the controlled coverage, the improvement degree of fatigue strength was similar to high-frequency mechanical impact (HFMI) treatment proposed in the IIW recommendation. On the other hand, it is obvious that the different treatment condition of shot peening influence the resulting compressive residual stress field and the degree of fatigue strength improvement. While the shot peening conditions in the previous studies [6-8] were based on empirical knowledge and experimental works, there remains a need to determine an optimal treatment condition based on a relationship between the condition and induced compressive residual stress. This is very crucial for developing a solid treatment criterion to ensure a high fatigue strength improvement for welded joints in actual steel bridges.

To effectively establish such a relationship, numerical modelling and simulations of the shot peening process have received interests for a long time. The previous study [9] developed a three-dimensional (3D) dynamic finite element (FE) method of shot peening and revealed the role of process parameters, such as shot velocity, shot size/shape, and the impact distance between two shots, in the induced residual stress distribution. In the study by Gualiano. 2001 [10], the developed 3D FE model on shot peening was utilized to link the residual stress induced in SAE1070 with a quality control indication, Almen Intensity. A recent study by Wang et al. 2019 [11] employed 3D shot peening model for 42CrMO and optimized the treatment parameters for the minimum compressive residual stress, compression layer depth, and stress concentration factor. The study experimentally verified the fatigue strength improvement for the material treated by the optimized parameters. The studies by Meo et al. 2003 [12] and Ikushima et al. 2017 [13] performed two-process approaches including thermal welding and dynamic shot peening simulations for Aluminum 1045 or SUS316. They presented the validity of simulated residual stress through comparison with experimental measurements. Barianayan et al. 2013 [14] tackled the numerical estimation of residual stress for shot peened cruciform welded joints using ASTM A572 steel and applied it to the fatigue life calculation using fracture mechanics. From above, the numerical simulation framework of shot peening has been established especially for base materials. The simulations can clarify the influence of multiple treatment parameters without extensive experiment work, correlating the simulation results with quality control. However, the simulation cases

and validations for welded joints, where introduced compressive residual stress in weld toes is crucial, are still limited. Thus, a practical and efficient numerical simulation system for estimating induced residual stress in welded large structures, especially steel bridges, is not yet developed.

Shot velocity is one of the essential parameters in shot peening simulations, as it directly influences the kinetic energy for shot impact and subsequent plastic deformation, thereby the residual stress field. In this regard, plenty of studies has been conducted to obtain the shot velocity. Some have indirectly measured and predicted shot velocity from clues such as indents and dimples resulting from shot media impingement [15, 16]. Such indirect measurement is a very simple approach, while it might be a challenge for targets with complex geometry like welded joints. Alternatively, the utilization of a high-speed camera has gathered attention as a more direct velocity measurement [17-19]. Ogawa et al. 1994 [17] used a high-speed shutter television camera to measure projected shot media under various conditions. The study presented a relevance of conditions such as shot diameter, shot density, and air-pressure on shot velocity. Recently, Ohta et al. 2021 [19] directly recorded shot movement in pneumatic shot peening. The impact of air pressure was discussed in terms of average shot velocity and shot velocity distribution for the shot flow cross-section. Furthermore, the study performed FE analysis of shot peening simulation reflecting the measured shot velocity and demonstrated well agreement between simulation and experimental results for induced residual stress. Thus, to obtain an accurate model for residual stress estimation for welded joints, understanding of actual shot velocity through direct measurement and its integration with numerical simulations are essential.

Therefore, this study experimentally performed direct measurements of shot velocity using an ultra-high-speed camera. Two nozzle types and distances between nozzle and specimen were prepared. Shot velocity was measured from shot movement captured by image processing. Then, a numerical simulation of shot peening was conducted using the explicit dynamic FE method, RADIOSS. The validation of its simulation was verified by comparison with previous studies [20, 21]. Parametric analysis and multiple shot peening analysis were undertaken to reveal key affecting factors in the simulations [21]. Based on the validated model and findings, the simulation model of shot peening for a steel plate was developed. The model reflected the direct shot velocity measurement results. Aiming to make better residual stress estimation for welded joints, the simulation model with measured shot velocity was used to study the influence of shot angle, friction coefficient, and material hardening rule on compressive residual stress distributions. These simulation outcomes were compared to the residual stress measurement results obtained near weld toes from previous studies [7, 8].

2. Direct shot velocity measurement

2.1. Measurement method and image processing

Figure 1 shows the ultra-high-sped camera, MEMRECAM Q1m, used for direct shot velocity measurement. This camera is capable of shooting at 2000 frames per second with a high resolution of 1280 × 1024 pixels. Figure 2 shows the setup for direct shot velocity measurement. The target specimen for measurement is a steel plate with welded gusset. To avoid camera damage from collision of projected shot media during shot peening, an acrylic plate was set in front of the camera and placed 3 m away from the specimen. The color of acrylic plate was clear and colorless enough to assume less influence on shooting picture quality. Moreover, two LED lights were used to ensure enough amount of light for clear shooting. Shot movements were captured with a shutter speed of 1/5000 second and a frame rate of 3000 fps. As in Figure 3, the shape of nozzle for shot peening was straight or curved ones. Shot distance between the nozzle and specimen was chosen to be 80 and 160 mm. The variations



Fig. 1 Ultra-high-speed camera

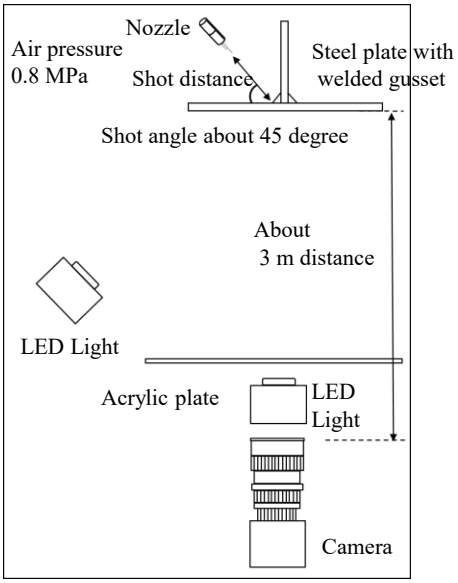


Fig. 2 Setup for shot velocity measurement



a Straight nozzle



b Curved nozzle

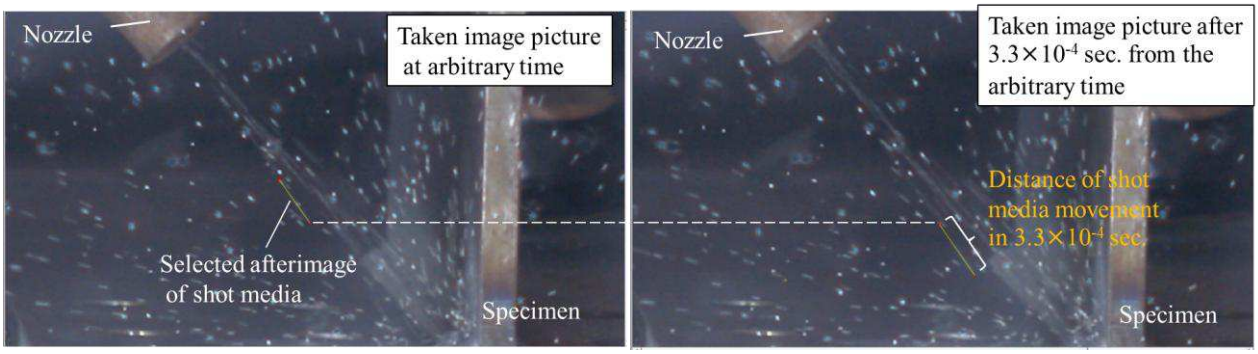
Fig. 3 Different nozzle shapes used for shot peening

in nozzle and distances aim to investigate their influence on shot velocity. Shot peening was performed using spherical steel shots (RCW10PH) whose diameter is 0.8 to 1.0 mm. The nozzle was directed at the weld with 45 degree and air pressure was 0.8 MPa. Figure 4 exemplifies the image pictures taken in the direct shot velocity measurement. Despite using two LED lights, the image clarity was limited, which makes it difficult to confirm the shot media sharply. Alternatively, it was possible to identify afterimages of the shot media on the image picture. Hence, shot velocity measurement relied on image processing without increasing in the frame rate of camera. The image processing used a software, MEMORICOM HXLink. An actual length per 1 pixel was determined based on the known nozzle diameter captured in the picture, which allows for scale conversion. The moving distance of 50 shot media within 0 to 40 mm distances from the specimen per frame (i.e., 3.3×10^{-4} sec in this investigation) were calculated for shot velocity measurement, as shown in Fig. 4.

2.2. Measurement results

Figure 5 shows the results of direct shot velocity measurement. Across all cases, the results indicated that the distribution of shot velocity was similar to a normal distribution shape. For the straight nozzle at 80 mm distance, many of shot velocity was around 60 m/s. Conversely, increasing the shot distance to 160 mm led to a shift in the distribution towards higher shot velocities, with the

majority around 90 m/s. For the curved nozzle, there is slight difference in 80 mm and 160 mm distances, but many of shot velocity was around 60 m/s which is the same as the straight nozzle at 80 mm distance. In summary, this measurement finds dominating measured velocities around 60 m/s, and this velocity is well consistent with the one generally stated in reference [e.g.,15]. On another note, one might anticipate that shot velocities decrease as shots approach the weld toe, while this measurement shows that the velocities rather increase with longer distances in the case of straight nozzle. The reason for this variation might be the fact that the straight nozzle directly transmits air pressure to shot media and maintains shot acceleration even at 160 mm distance. However, this clarification needs further investigation due to limited cases examined in this study. It is also necessary to seek methods that keep a constant distance as much as possible during construction in bridge construction sites. Figure 6 shows the relationship between air pressure and shot velocity. This study's



a Direct shot velocity measurement by image processing



b Straight nozzle, 65 m/s

c Straight nozzle, 105 m/s

Fig. 4 Example of image picture taken in the direct shot velocity measurement

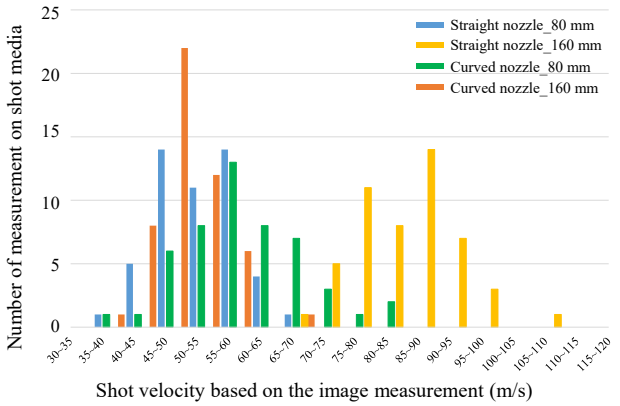


Fig. 5 Direct shot velocity measurement results

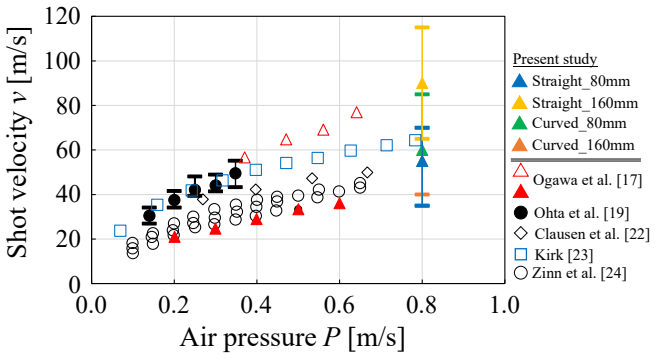


Fig. 6 Comparison of relationship between air pressure and shot velocity

results for each case are presented as average values together with scatter band representing max and min values. The figure also includes the results from previous studies [17, 19, 22-24] for comparison. From the figure, there is clear trend that the shot velocity increases according to increase in air pressure. The measurement results in this study were well within the trend found in the existing literature. Therefore, this study confirms the validation of shot velocities obtained by image processing. The shot velocities in this study can be utilized for numerical simulations.

3. Numerical simulation of shot peening

Towards developing the numerical simulation of shot peening for welded joints, this chapter focuses on three fundamental analyses: single shot analysis, parameter analysis, and multiple shot analysis for 3D material plate models. The single shot analysis aims to validate analysis model by comparison with previous studies [10, 25]. In addition, an efficient model with reasonable accuracy and less computation time are studied. In parameter analysis, various parameters such as model size, material properties, and shot velocity are examined based on the single shot model. The multiple shot analysis confirms the influence of multiple shot impacts on introduced compressive residual stress.

3.1. Simulation method for single shot peening

Figure 7 shows an analysis model of single shot peening. Numerical simulations were conducted using RADIOSS explicit finite element commercial code that solves the non-linear dynamic problem. This model referred to a previous study [10]. The distance between the target and the center of shot was 1.2 mm. This distance did not affect the numerical results as the acceleration of gravity was not given the model. The modelling for the target considered 8-node solid elements with 8 gauss integration points, which is recommended by the RADIOSS, while for the shot, the same 8-node solid element but with 1 gauss integration point. To model the local response in shot impact region sufficiently, a refined element with a minimum of 0.04 mm was applied to the center top region affected by the shot impact, gradually increasing towards the plate edge. Only the nodes at the bottom of target were constrained to the displacement in the z-direction as the boundary condition.

Table 1 shows the material properties of modelled targets and shots. The shots were considered two types of properties: either stainless steel (SUS304) or rigid. Figure 8 shows the stress-strain curves for the target and shot, having bilinear slope with 0.1 % of Young's module. As the previous study [10] did not clearly state the yield strength of stainless steel, the value was determined with reference to another study [12] which presents the results of subsequent study by the research group that conducted the previous study [10]. This study considered the Johnson-Cook material model as implemented in RADIOSS. The model can be described as the following equation.

$$\sigma = \left(a + b \cdot \varepsilon_p^n\right)\left(1 + c \cdot ln\frac{\dot{\varepsilon}}{\dot{\varepsilon}_0}\right) \quad (1)$$

where, a is yield strength, b and n are hardening coefficient, ε_p is plastic strain, c is strain rate coefficient, $\dot{\varepsilon}$ is strain rate (s^{-1}), and $\dot{\varepsilon}_0$ is reference strain rate (s^{-1}). Since this study used bi-linear curve, n value was 1.0 and b value was equal to the curve slope after yielding. This chapter did not consider strain rate sensitivity during the shot peening process. A material hardening rule can be manually defined by setting a numerical character, C_{hard} parameter, which ranges from 0.0 to 1.0 [26]. A value of C_{hard} = 0.0 is isotropic hardening, while C_{hard} = 1.0 is the kinematic Prager-Ziegler hardening model. Intermediate values between 0.0 and 1.0 correspond to hardening behavior between the above

two models, i.e., combined isotropic and kinematic hardening. This chapter employed C_{hard} = 0.0. The Mises yield criterion was used for a yield criterion.

The shot velocity was set at 60 m/s. The contact condition was RWALL in the model for rigid shot. This condition provides a contact constraint that acts on the slave nodes, preventing from penetrating nodes into the wall. When the contact is detected, the acceleration and velocity of the slave are modified. The model having the shot of SUS304 employed the penalty method based on master/slave treatment. The surface of shot was defined as a master segment, while the surface of target

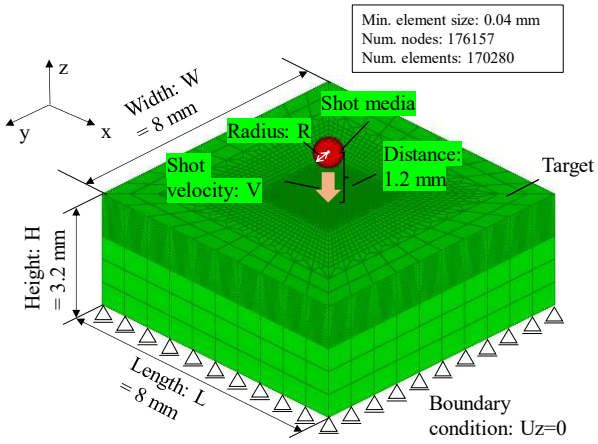


Fig. 7 Single shot peening model

Table 1 Material properties
(SUS316, SUS304, Rigid)

Material property	SUS316L	SUS304 (Shot)	Rigid (Shot)
Density (g/cm^3)	7.92	7.9	7.9
Young's module (MPa)	194700	198500	
Poison's ratio	0.285	0.294	
Yield stress (MPa)	231	288	
Strain hardneing coefficient (MPa)	2427	1474	

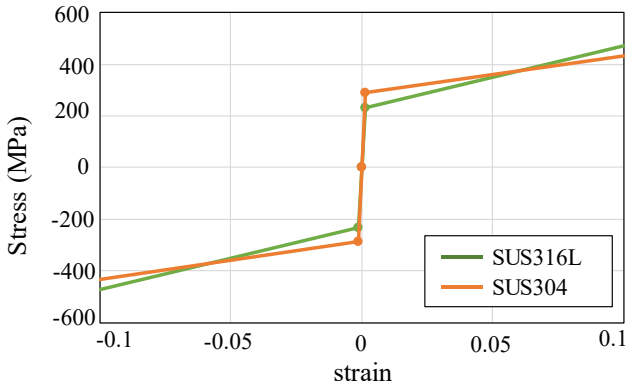


Fig. 8 Stress-strain curve for SUS316L, and SUS304

was designated as a set of slave nodes. The friction coefficient between the shot and target was 0.15. Strain rate and damping were not considered. The courant condition was used as the time increments.

3.2. Simulation results of single shot peening

Figure 9 shows the residual stress distributions through the thickness for the simulation results from this study and previous studies. These distributions are extracted from the bottom of shot indent toward the depth direction; see right pictures in Fig. 9. The distributions obtained in this study showed a similar trend to the previous studies where the tensile residual stress was introduced near the surface, transitioning to compressive residual stress at sub-surface, with its decreases in magnitude as depths increase. Comparing the simulation results between the elastic model in the previous studies and the rigid shot model in this study, the depth at which residual stress became zero (i.e., the depth of compression layer) was slightly different, but the peak values of compressive residual stress were in good

agreement. Comparing the analysis results of different shot models in this study, the peak values of compressive residual stress were almost the same, but the depth of compression layer for the SUS304 shot was shallower than that for the rigid shot. For this reason, the previous study [27] stated that in case of elastic-plastic material assumption for shots, the plastic deformation of shot media absorbed the energy in collision, which reduces the area of compressive residual stress field. Similar result is observed in this study as shown in Fig. 9. Despite this slight difference, the computational cost for the SUS304 shot was about 2.5 times higher than that for the rigid shot. As a result, the above simulation

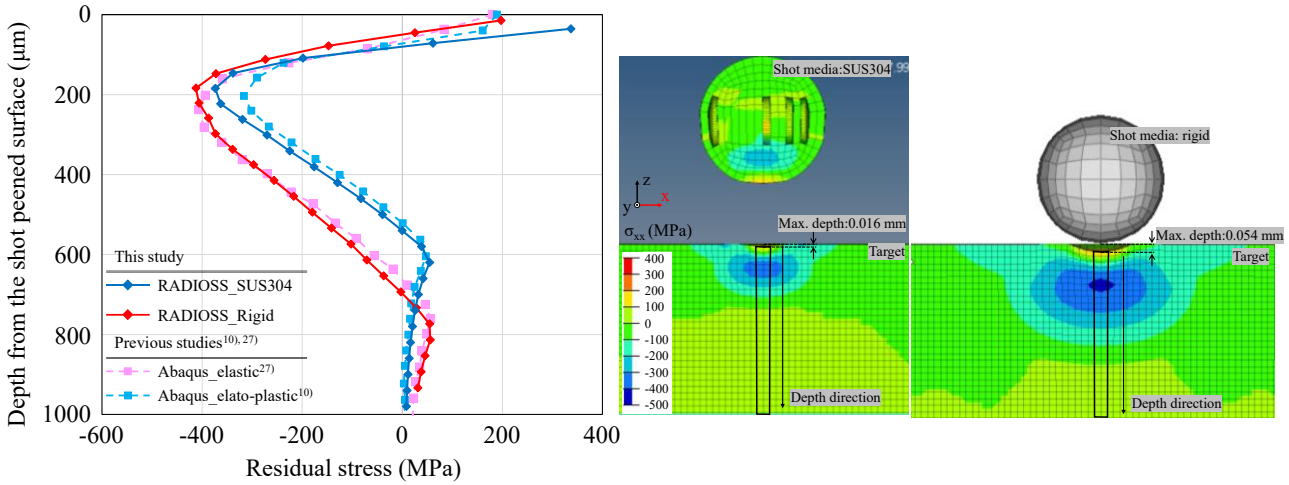


Fig. 9 Simulation results of single shot peening

results and comparisons indicated the validity of simulation model in this study and the possibility of running efficient analysis with certain accuracy by using the rigid shot.

3.3. Parametric analysis on model size, material properties, and treatment conditions

To investigate the effects of various model sizes, material mechanical properties, and shot peening treatment conditions on the residual stress distribution, a parametric analysis was carried out on the same model using the rigid shot in Fig. 7, as validated in **Section 3.2**. The parameters were the following: length L (mm), height H (mm), material yield strength Y (MPa), Young's modulus E (MPa), Poisson's ratio ν, shot velocity V (m/s), shot volume M (mm^3), and shot radius R (mm). Table 2 shows a list of parameter analysis. The values of the parameter are largely variable to investigate the effect of each parameter; thus, note that some are not the realistic values.

3.4. Results of parametric analysis

Figure 10 shows the results of the parametric analysis. First, different model sizes for length (L) and height (H) of target material were analyzed to investigate the influence of model dimension, as shown in Figs. 10**a** and 10**b**. As a result, L mainly affects the peak value of compressive residual stress, and it converges more than 4.0 mm. H has little impact on the residual stress distribution unless extremely thin value with less than 0.2 mm. After these results, the following analysis for other parameters was based on the model size with 8.0 mm length and 3.2 mm height.

Second, the material mechanical properties of target model are variable parameters to confirm their sensitivities in induced residual stress distributions, while shot peening conditions are fixed. In Fig. 10**b**, as the yield stress (Y) increased, the peak value of compressive residual stress increased, and the depth of compression layer became smaller. Under a relatively lower shot velocity of 32 m/s, the

Table 2. List of parameters considered in the analysis

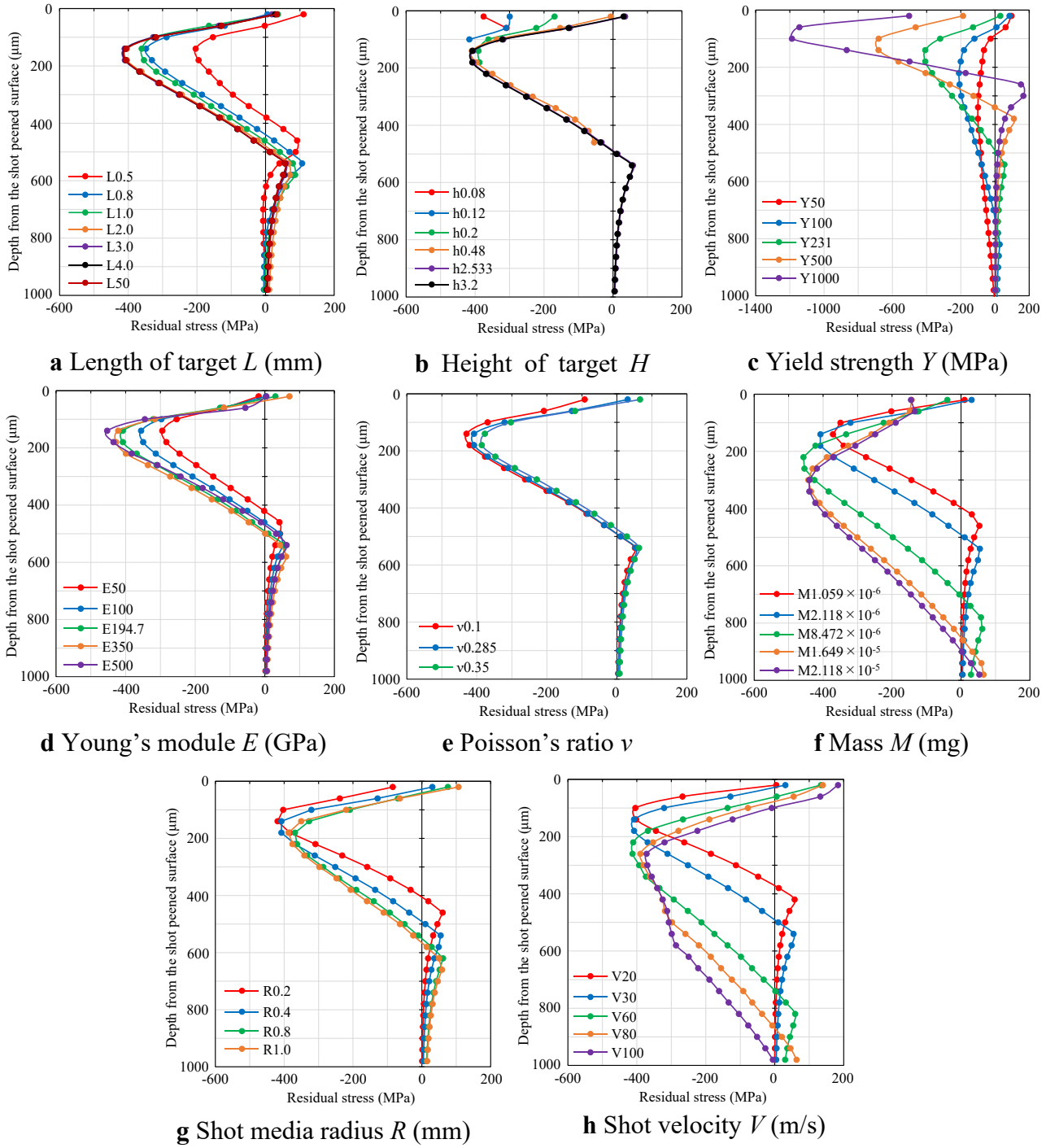
Parameters		Scale factor	L (mm)	H (mm)	Y (MPa)	E (GPa)	ν	M (mg)	R(mm)	V (m/s)
			8	**3.2**	**231**	**194.7**	**0.285**	**2.118**	**0.4**	**30**
(a)	Length of target: L (mm)	L-0.0625	**0.5**	3.2	231	194.7	0.285	2.118	0.4	30
		L-0.1	**0.8**	3.2	231	194.7	0.285	2.118	0.4	30
		L-0.125	**1**	3.2	231	194.7	0.285	2.118	0.4	30
		L-0.25	**2**	3.2	231	194.7	0.285	2.118	0.4	30
		L-0.375	**3**	3.2	231	194.7	0.285	2.118	0.4	30
		L-0.5	**4**	3.2	231	194.7	0.285	2.118	0.4	30
		L-6.25	**50**	3.2	231	194.7	0.285	2.118	0.4	30
(b)	Height of target: H (mm)	h-0.025	8	**0.08**	231	194.7	0.285	2.118	0.4	30
		h-0.0375	8	**0.12**	231	194.7	0.285	2.118	0.4	30
		h-0.0625	8	**0.2**	231	194.7	0.285	2.118	0.4	30
		h-0.15	8	**0.48**	231	194.7	0.285	2.118	0.4	30
		h-0.7915	8	**2.533**	231	194.7	0.285	2.118	0.4	30
(c)	Yeild Strength: Y (MPa)	Y-0.2164	8	3.2	**50**	194.7	0.285	2.118	0.4	30
		Y-0.4329	8	3.2	**100**	194.7	0.285	2.118	0.4	30
		Y-2.1645	8	3.2	**500**	194.7	0.285	2.118	0.4	30
		Y-4.3290	8	3.2	**1000**	194.7	0.285	2.118	0.4	30
(d)	Young's Modulus (GPa)	E-0.2568	8	3.2	231	**50**	0.285	2.118	0.4	30
		E-0.5136	8	3.2	231	**100**	0.285	2.118	0.4	30
		E-1.7976	8	3.2	231	**350**	0.285	2.118	0.4	30
		E-2.568	8	3.2	231	**500**	0.285	2.118	0.4	30
(e)	Poisson's ratio: ν	ν-0.3508	8	3.2	231	194.7	**0.1**	2.118	0.4	30
		ν-1.228	8	3.2	231	194.7	**0.35**	2.118	0.4	30
(f)	Mass: M (mg)	M-0.5	8	3.2	231	194.7	0.285	**1.059**	0.4	30
		M-4	8	3.2	231	194.7	0.285	**8.472**	0.4	30
		M-8	8	3.2	231	194.7	0.285	**16.94**	0.4	30
		M-10	8	3.2	231	194.7	0.285	**21.18**	0.4	30
(g)	Shot media redius: R (mm)	R-0.5	8	3.2	231	194.7	0.285	2.118	**0.2**	30
		R-2	8	3.2	231	194.7	0.285	2.118	**0.8**	30
		R-2.5	8	3.2	231	194.7	0.285	2.118	**1**	30
(h)	Shot velocity: V (m/s)	V-0.667	8	3.2	231	194.7	0.285	2.118	0.4	**20**
		V-2	8	3.2	231	194.7	0.285	2.118	0.4	**60**
		V-2.667	8	3.2	231	194.7	0.285	2.118	0.4	**80**
		V-3.333	8	3.2	231	194.7	0.285	2.118	0.4	**100**

model behaves an elastic body with increased *Y* values. Consequently, there is reduction in the amount of plastic deformation due to shot collision. As Fig. 10**c** indicate, the increases of Young' modulus (*E*) brought about the increase of the peak value of compressive residual stress and the depth of compression layer. The influence of Poisson's ratio (*v*), shown in Fig. 10**d**, was not significant. From above, as can be expected, the material and its yield strength greatly change the introduced residual stress field.

Physical parameters related to shot peening conditions, shot mass, shot radius, and shot velocity, were arbitrarily changed to understand how these changes influence the introduced residual stress distributions. In Fig. 10**f**, increase in the shot mass (*M*) tended to increase the peak value of compressive residual stress and the depth of compression layer but these converged in the case of shot velocity was constant. With the increase of shot radius (*R*) and velocity (*V*), in Figs. 10**g** and 10**h**, the peak value of compressive residual stress became slightly smaller, while the depth of the compression layer became deeper. Important feature observed is that certain compressive residual stress can be introduced despite some variations in shot velocities. Therefore, the results imply that the combination of low and high shot velocity might generate certain compressive residual stress near subsurface, at the same time making compression layer deeper.

When it comes to the actual steel, *E* and *v* should be almost constant values of around 200 GPa and 0.3, respectively. Thus, the *E* and *v* do not make a significant difference to residual stress. In addition, material yield strength is generally determined according to the type of steel, thereby the

change of the amount of introduced residual stress depends on the shot peening processing condition. For example, if one needs larger compressive residual stress, the mass of shot will be increased. If one needs deeper compression layer depth, the velocity, mass and radius of shot will be increased.



a Length of target L (mm) **b** Height of target H **c** Yield strength Y (MPa)

d Young's module E (GPa) **e** Poisson's ratio v **f** Mass M (mg)

g Shot media radius R (mm) **h** Shot velocity V (m/s)

Fig. 10 Results of parametric analysis

Therefore, to ensure the prescribed amount of compressive stress and depth of compression layer, the velocity, mass, and radius of shots must be controlled certainly in the actual shot peening processing.

3.5. Simulation method for multiple shot peening

This section deals with numerous shot impacts as more representative of the actual shot peening process. Specifically, multiple shot peening analysis was conducted to investigate the effects

of the relative position of the shots on the residual stress distribution. The dimensions and material properties of the analysis model were referred to the model in a previous study [25]. Figure 11 shows the simulation model for the multiple shot peening. The model was represented as an aluminum alloy with $H = 5.1$ mm, $L = 15$ mm, and $W = 15$ mm. The shot diameter was 2.36 mm. The distance between the target and the center of the shot was 3.5 mm. A minimum element size of 0.125 mm was allocated around the center top on which the multiple shots are impacted. Please note herein that the minimum element size and dimensions of target and shot are different from the model for single shot analysis in **Section 3.2**. However, this element size corresponds to the one often used for numerical simulation of HFMI [e.g.,28], thus considered small enough. Also, the target model's dimension is confirmed to be large enough not to influence the numerical results as shown in **Section 3.4**. Table 3 and Figure 12 show the material properties and stress-strain curves for the modelled plate and shot, respectively. The strain hardening coefficient with 0.1 % of Young's modulus. The shot velocity was set at 32 m/s [25].

This study performed three simulation cases. As first case, the impact position of second shot varied. The first shot impact was at the center top, where the coordinate is defined as $x = 0$, then the second shot was followed toward the x-axis. The distance between two shots, D was eight different ways: D = 0, 0.1R, 0.2R, 0.3R, 0.4R, 0.5R, 0.75R, and R (where R is the shot radius of 1.18 mm). As second case, three shots were impacted at the same position, D = 0. As last case, the function was both the number of shots (three to six shots) and impact position. For three shots, the impact position is D = 0, 0.1R, 0.2R, similarly, for four shots, D = 0, 0.1R, 0.2R, 0.3R, and for five shots, D = 0, 0.1R, 0.2R, 0.3R, 0.4R, and for six shots, D = 0, 0.1R, 0.2R, 0.3R, 0.4R, 0.5R. As shown right hand size of Fig. 11, residual stress distributions were extracted at both first and the second shot impact positions in the

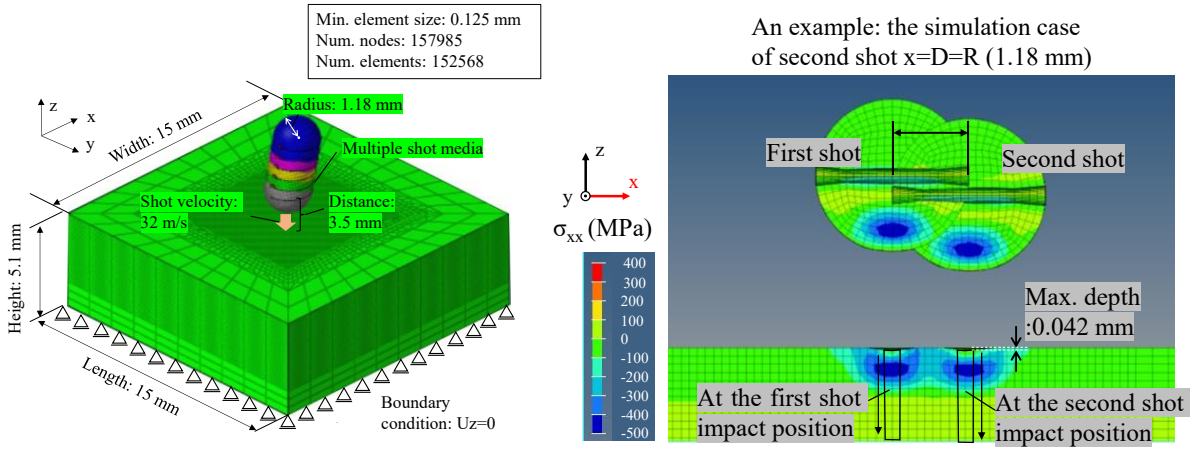


Fig. 11 Multiple shot peening model

Table. 3 Material properties for 7075-T6 and shot

Material property	7075-T6	Shot
Density (g/cm³)	2.8	7.9
Young's module (MPa)	74430	198500
Poisson's ratio	0.33	0.294
Yield stress(MPa)	578	650

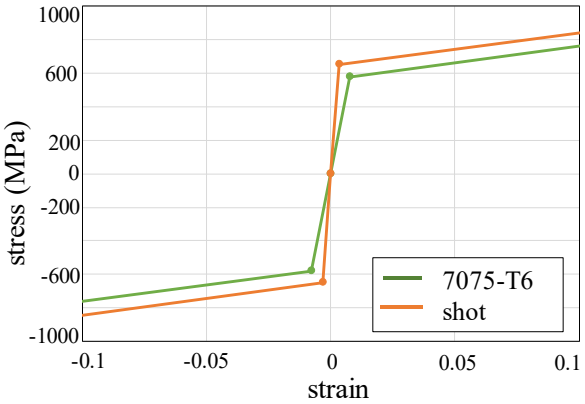


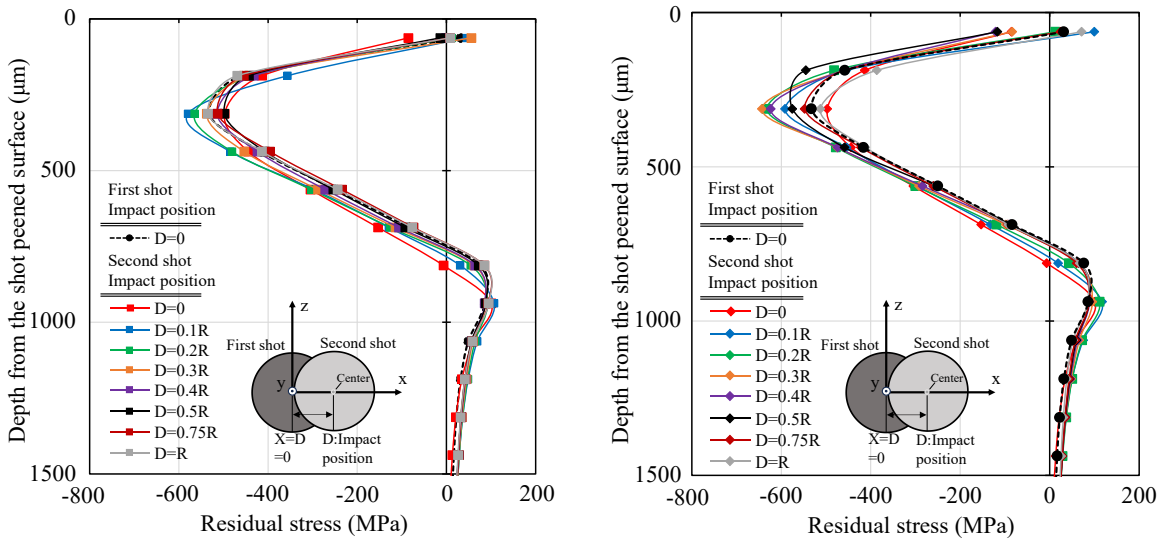
Fig. 12 Stress-strain curve for 7075-T6 and shot

first case, but in other two cases, the distribution at first one was only confirmed.

3.6. Simulation results for multiple shot peening

Figures 13 to 15 show the results for first to third simulation cases. From Fig. 13, the influence of second shot and its position in a function of D can be seen particularly for the peak value of compressive residual stress induced by the first shot. In Fig. 13**a**, positioning the second shot at D = 0 or 0.3R to R slightly increased the peak value or made it unchanged. There was about 100 MPa increase when second shot was located at either D = 0.1R or 0.2R. In Fig. 13**b**, the results for second shot positioned at D = 0.1R to 0.5R exhibited the larger peak values compared to the first shot, and the most influencing position was D = 0.3R. As Fig. 14 shows, when the second shot was applied to the exact same position as first shot, the peak residual stress became smaller, but the depth of the compression layer became deeper. The subsequent third shot led to the similar residual stress distribution to that of the second shot. In Fig. 15, additional shot impacts in the interval of 0.1R in the x-axis contributed to slightly raising the tensile residual stress on the surface of the target. However, the shape of residual stress distribution was almost the same.

From above, the amount of introduced residual stress changes according to impact position after the second shot. Multiple shot impacts are found favorable to the introduced compressive residual stress, especially when the distance of subsequent shot impact position is less than around 0.2R. This condition shows the increase of peak compressive stress, about -100 MPa. However, more than 0.2R, the interaction effect of multiple shots become gradually smaller. Thus, the effect of actual shot peening on introduced compressive residual stress field might be converged to be constant.



a. Residual stress distribution at first shot impact position

b. Residual stress distribution at second shot impact position

Fig. 13 Results of first simulation case: influence of second shot position

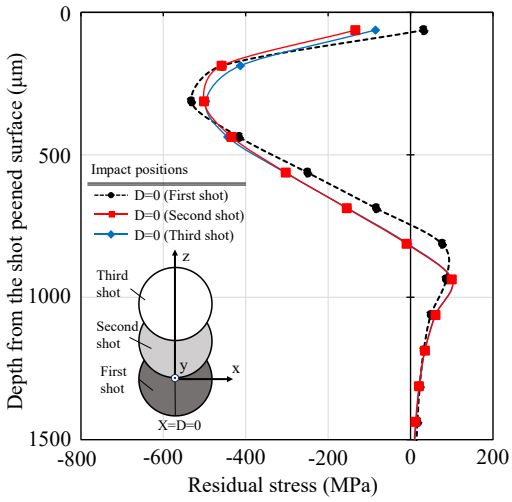


Fig. 14 Results of second simulation case: influence of second and third shot at the same position as first shot

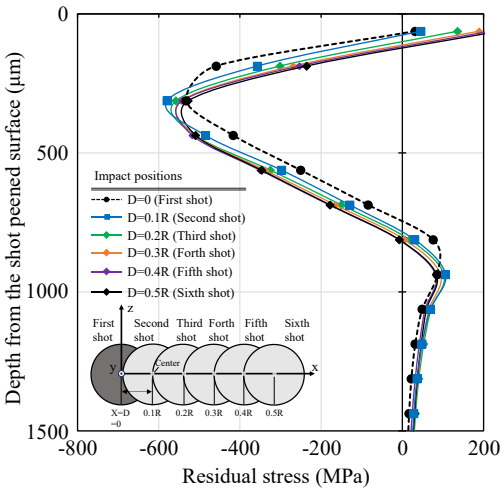


Fig. 15 Results of third simulation case: influence of third to sixth shot position

4. Comparison between simulation and experiment results reflecting shot velocity measurement

This chapter presents simulation results for shot peening applied to a steel plate, comparing them with residual stress measurements obtained near weld toes in existing steel bridges. The model incorporates the shot velocity directly measured in **Section 2**. Towards developing better residual stress estimation for welded joints, this chapter also focuses on the influence of material hardening rules, shot angle, and friction coefficient on the simulated residual stress and comparison results.

4.1. Simulation model of shot peening for a steel plate

Figure 16 shows simulation model for residual stress estimation in welded joints. This study made a steel plate model without the weld and gusset plate, as developed and validated in **Section 3**. For this reason, the residual stress measurements for comparison have been conducted on steel plates being 2 mm away from weld toes [21]. At this location, the residual stress value and compression layer depth was nearly identical, irrespective of the presence of welds and gussets [21] According to previous studies, the shot diameter was set at 0.9 mm. This refers to the real diameter of shot media, 0.8 - 1.0 mm. The shot steel is RCW10PH, modelled as rigid body based on **Section 3.2**. Only single shot was applied. The shot velocity varied from 35 to 130 m/s reflecting the results in **Section 2.2**. This chapter systematically investigated different shot angles, spanning from 15 to 90 degrees, to understand their effects on introduced compressive residual stress distribution. In the manual shot peening like Fig. 3, despites efforts to keep a constant nozzle angle, variations in shot angle are unavoidable. Thus, shot media is assumed to hit the surface not only at a fixed angle but also at various angles. Along with different shot angle, the variable friction coefficient was considered either no friction, 0.2, 0.5 or 1.0. Dynamic friction between a surface impacted by a shot is known to be an important factor, and this friction's influence is numerically defined by friction coefficient. Researchers often provided friction coefficient in the range from no friction to 0.4 [9, 11, 12, 19] from engineering perspective. Literature review by Schulze et al. [29] states that the influence of friction coefficient on residual stress

distribution is significant when shot angle is under 75 degrees. Table 4 and Figure 17 show material properties and stress-strain curve, respectively. The yield stress was defined as 434 MPa. In addition to isotropic hardening (C_{hard}=0.0), the combined (C_{hard}=0.5) and kinematic hardening models (C_{hard}=1.0) were also selected. Rahamaan et al. [30] reported that deformation resistance is low dependence with strain rate up to 100 s^{-1} on A7075-T6 aluminum alloys at room temperature. However, our target is low carbon steel. Hence, the strain rate was defined as either no consideration, or 100 s^{-1}, confirmed its strain rate dependency. The strain rate coefficient, c, in equation (1) is significantly influenced by strain rate of tensile test. Hence, the c value was arbitrarily chosen as either 0.0054 or 0.0247. The former and letter were taken and calibrated by the studies by Yadav et al. [31] for mild steel tested by strain rates on the range from 0.06 to 1.0 s^{-1} and by Forni et al. [32] for S355 steel tested by strain rates on the range from 5 to 850 s^{-1}.

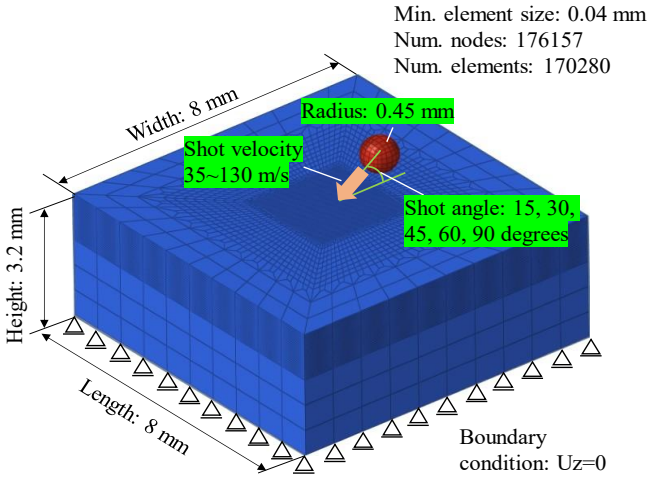


Fig. 16 Simulation models for residual stress estimation in welded joints

Table 4. Material properties for SM490YA and RCW10PH

Material property	SM490YA	Rigid (Shot)
Density (g/cm^3)	7.85	7.9
Young's module (MPa)	200000	
Poison's ratio	0.3	
Yield stress (MPa)	434	

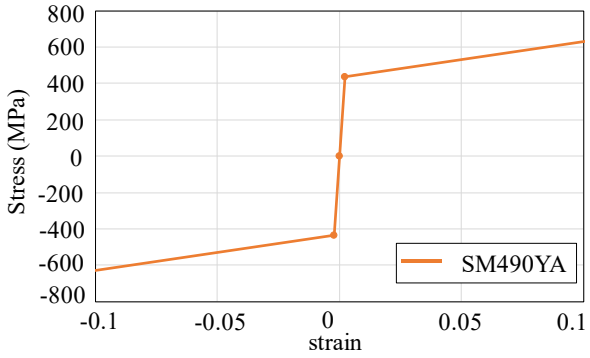
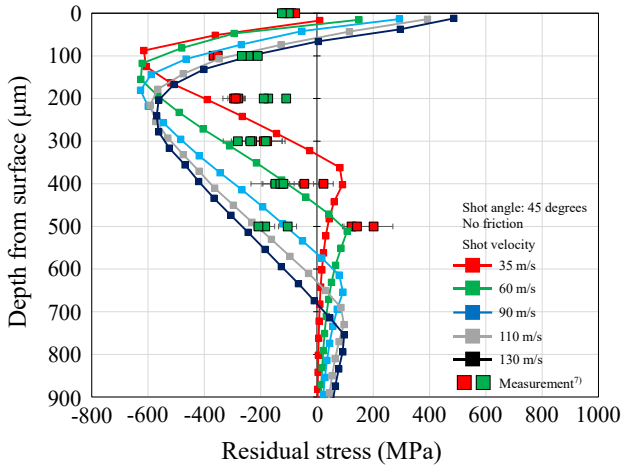


Fig. 17 Stress-strain curve for SM490YA

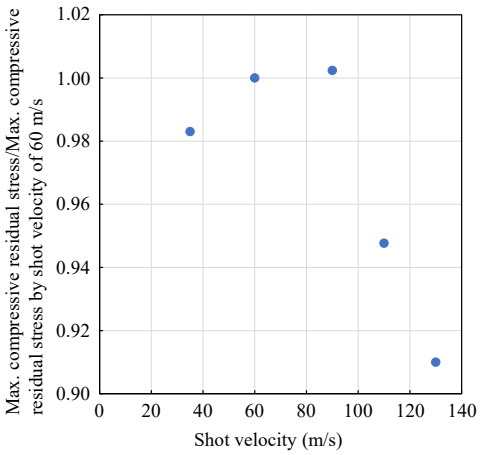
4.2. Comparison results between numerical simulations and experiments

Figure 18 shows the comparison of numerical and experimental results for residual stress distributions. These simulation results are in function of shot velocities, while other parameters are fixed. In the simulation, the influence of shot velocities was significant for compression layer depth, while minor for peak residual stress value and its depth. From Fig. 18**a**, increases in shot velocity led to a deeper compression layer, the same trend as the parameter analysis, as shown in Fig. 10**h.** The depth of compression layer was comparable with the experimental one. In particular, the numerical

results for 60 m/s showed well match in not only the depth of compression layer but the depth of peak compressive residual stress, which are around 500 μm and 100 μm, respectively. From above, the shot velocity of 60 m/s, frequently observed in the direct measurement, enables to capture well the depths of minimum compressive residual stress and plastic region. In Fig. 18**b**, the minimum value of compressive residual stress was normalized with the one by 60 m/s. Even though the shot velocity significantly varied from 35 m/s to 130 m/s, the change in the minimum value remained within 10%. However, across all the results, the peak value of compressive residual stress was larger than that for the experimental results. Thus, further improvements need to be addressed for estimation accuracy.



a Shot angle of 45 degrees and shot velocity varied from 35 to 130 m/s



b Normalized max. compressive residual stress based on shot velocity of 60 m/s

Fig. 18 Comparison of measurements and numerical simulation results

4.3. Influence of shot angle, friction, and material hardening rules on comparison results

Figure 19 presents the simulation results in relation to material hardening rules and strain rates. Excluding the effect of strain rate, the different hardening model changed the depth of peak value of compressive residual stress and the depth of compressive layer. However, the degree of change was not significant. The effect of strain rate on combined hardening model appeared especially near the shot peened surface for c= 0.0054 and around 200 μm depth for c= 0.0247, while slight difference is only seen on isotropic hardening model in both cases. However, the sensitivity of strain rate in this study is not much high in introduced compressive residual stress and its distribution. Thus, the change in hardening model is insensitive for residual stress distribution and the effect of strain rate on combined hardening model might be significant for residual stress near the shot peened surface but significantly depended on the c value.

Figure 20 shows the simulation results for different shot angles. The effect of friction was not considered. The shot angles of 45, 60, and 90 degrees indicated similar residual stress distributions. When the shot angle was less than 30 degrees, the peak compressive residual stress somewhat decreased and approached the experiments. However. the depth of peak value and compression layer gradually became shallower, which was inconsistent with the experiments. Figure 21 shows the cross-section profiles and stress contours in shot peened area. Plastic deformation by shot media, i.e., indent depth obviously depended on shot angle, with the deepest indent found by 90 degrees. From the stress

contour, the peak compressive residual stress always occurred along extension line of the shot angle, and its location was localized near the surface especially for 15 and 30 degrees. The affected area by plastic deformation became narrow as the shot angle decreased. Thus, the influence of different angles is significant when the shot angle is relatively low.

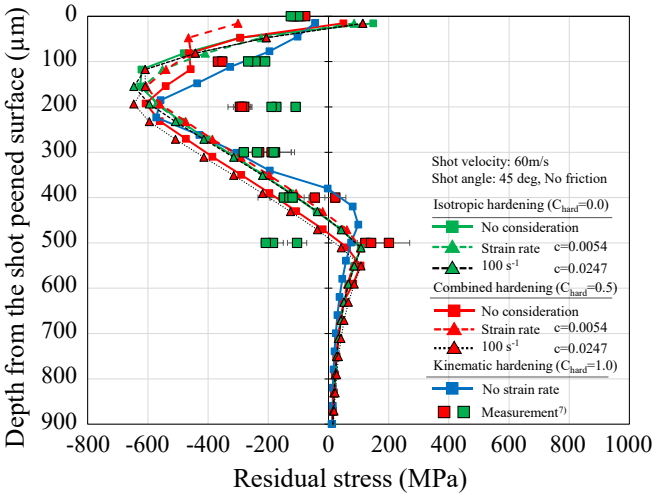


Fig. 19 Results of different hardening models

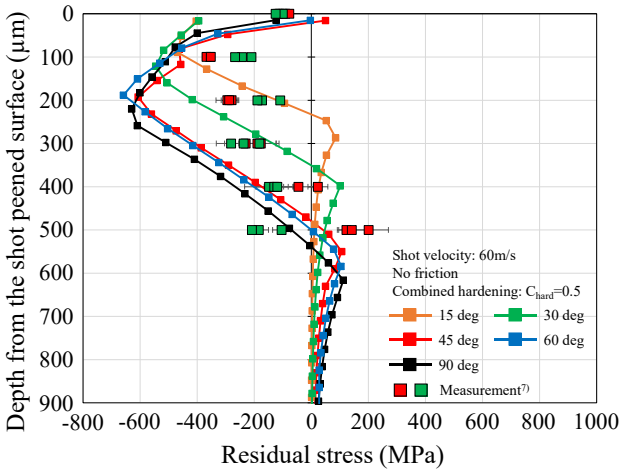


Fig. 20 Results for different shot angles

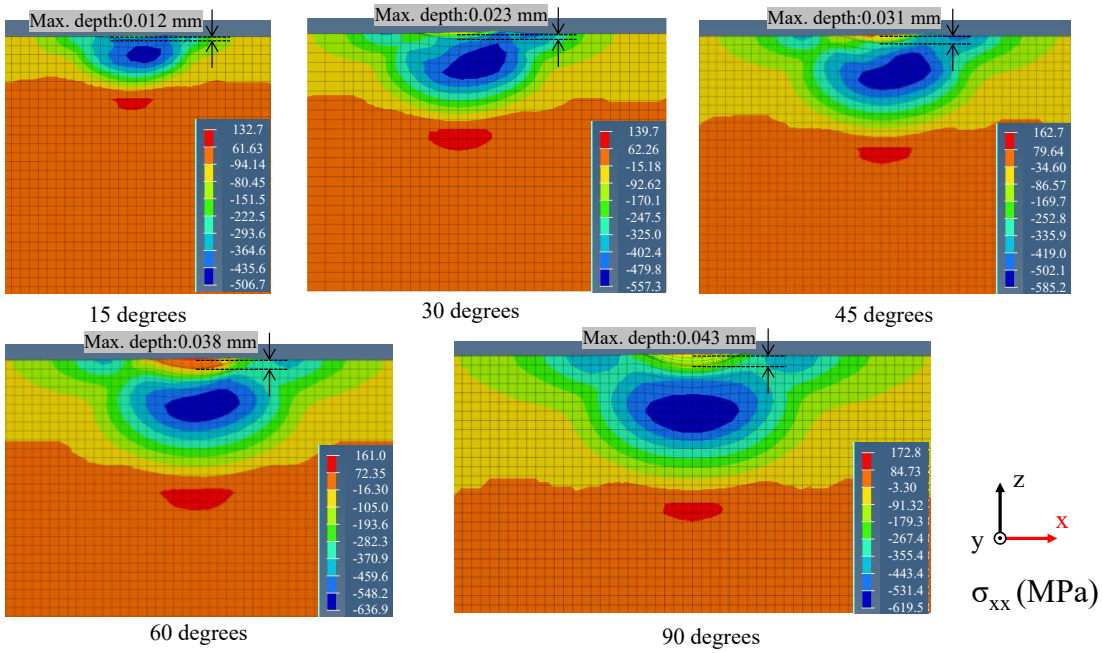


Fig. 21 Contour diagrams in function of different shot angle

Figure 22 shows the simulation results for different friction coefficients as a function of shot angle. The influence of friction coefficient can be observed, especially for the residual stresses near the treated surface. There was a clear trend that the peak value of compressive residual stress decreased with increasing in friction coefficient, while keeping the similar depth of compression layer. This trend was more apparent when the shot angle was smaller. Considering the friction coefficients, the compressive residual stress at the top surface for 15 and 30 degrees decreased, while tensile residual stress for 45 and 60 degrees turned into compressive side. As a result, the peak value of compressive residual stress and its depth gets closer to the experimental results in case of less than 45 degrees and consideration of friction. The reproducibility of simulated results is improved by accounting for the

combined effect of shot angle and friction. Therefore, the shot peening angle for weld toes needs to be certainly controlled.

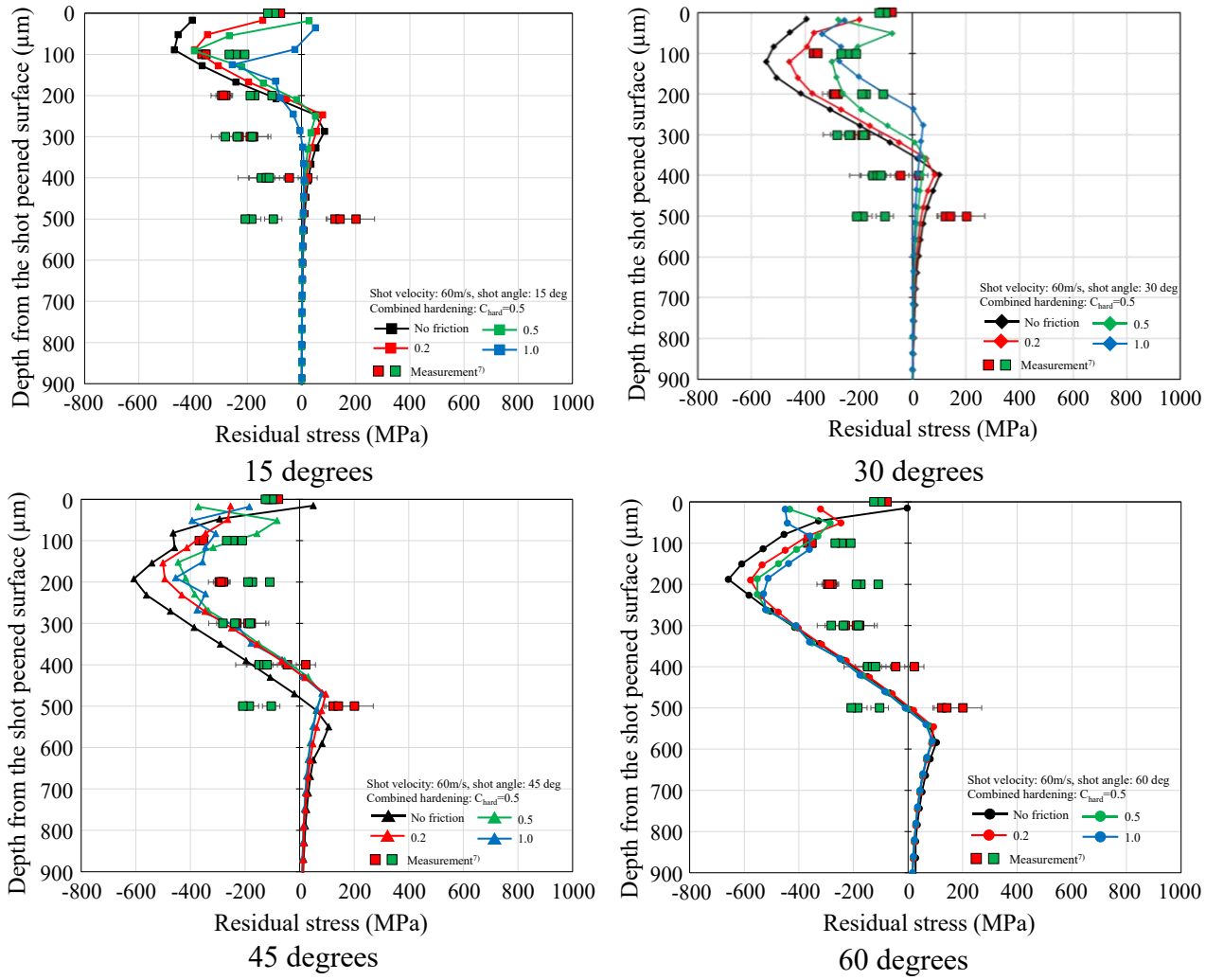


Fig. 22 Results of combination of different shot angle and friction coefficient

5.Conclusions

The following conclusions are drawn from this study.

1. Direct shot velocity measurement resulted in indicating 60 m/s, a value generally said in the previous study [15], despite the shot velocity increases with increasing the distance between the nozzle and the specimen in case of a straight nozzle.
2. For single shot peening analysis, the comparison of analysis results with a previous study on stainless steel indicated the validity for this analysis. Moreover, an efficient analysis model with less computation time and acceptable accuracy might be made by defining the shot material as a rigid or elastic body.
3. The results of parametric analysis showed that the residual stress distribution changed according to the shot peening processing conditions. In particular, the velocity, mass, and radius of shots needs to be controlled certainly to ensure the prescribed depth of compression layer and amount of compressive residual stress. In addition, the multiple shot impact may contribute to decreasing the introduced compressive residual stress and being converged to be constant.
4. The comparison of residual stress distributions from experimental measurements and numerical

simulations reflecting measured shot velocity on the steel plate showed better agreement with respect to the amount of the compressive residual stress and the depth of compression layer. Based on this simulation model, the shot angle and friction are found to affect the amount of compressive residual stress, so a certain control of shot peening angle to weld toes is essential.

The authors consider the following studies for future research. This study carried out multiple shot analysis with constant velocity, but there are some variations in velocities, as obtained in **Section 2**. Thus, the numerical simulation should be extended to account for multiple shots with random velocities and compared with experiments for further improvement of estimation accuracy. The simulation model in this study was based on a steel plate without welds and gussets, i.e., targeting a shot peened surface away from weld toes. Thus, random multiple shot simulations need to be implemented to welds for better understanding in how shots impact weld toes. A particular interest may be in developing a numerical simulation model for grit-blasting. Some studies experimentally investigate the combined effect of grit-blasting and peening on fatigue behavior of welded joints [34, 35]. Thus, this allows for the numerical investigation on the influence of surface roughness and residual stress e.g., on HFMI-treated welds.

Acknowledgement

The authors would like to acknowledge YAMADA INFRA TECHNOS Co., Ltd. for providing and conducting shot peening on the steel plate with welded gusset and assistant professor Takahiro Iwata in Aichi Institute of Technology (when he was a researcher in Gifu university) for helping to establish the numerical simulation model of shot peening.

References

1. Yokoyama, L., Miki, C. (2017) Participatory database of repair cases on fatigue damaged welded structures, International Journal of Fatigue, Vol.101, pp.358-396, https://doi.org/10.1016/j.ijfatigue.2017.01.010.
2. Huther, I., Lieurade, HP., Souissi, R., Nussbaumer, A., Chabrolin, B., Janosch, J-J. (1996) Analysis of results on improved welded joints, Welding in the World, Vol.37, No.5, pp.242-266.
3. Barsoum, Z., Jonsson, B. (2008) Fatigue assessment and lefm analysis of cruciform joints fabricated with different welding processes, Welding in the World, Vol.52, pp.93-105, https://doi.org/10.1007/BF03266657.
4. Hensel, J., Nitschke-Pagel, T., Dilger, K. (2016) Effects of residual stresses and compressive mean stresses on the fatigue strength of longitudinal fillet-welded gussets, Welding in the World, Vol.60, pp.267-281, https://doi.org/10.1007/s40194-015-0284-6.
5. Welsch, W.H. (1991) A Concept for Preventing Repeated Weld Repairs of Bridge Structures, ASTM International, pp. 208-226, https://doi.org/10.1520/STP14540S.
6. Kinoshita, K., Banno, Y., Ono, Y., Yamada, S., Handa, M. (2019) Fatigue Strength Improvement of Welded Joints of Existing Steel Bridges by Shot-Peening, International Journal of Steel Structures, Vol. 19, No. 2, pp. 495-503, https://doi.org/10.1007/s13296-018-0140-9.
7. Kinoshita, K., Ono, Y., Banno, Y., Yamada, S., Handa, M. (2020) Application of shot peening for welded joints of existing steel bridges, Welding in the World, Vol. 64, pp. 647-660, https://doi.org/10.1007/s40194-020-00863-w.
8. Kinoshita, K., Sugawa, K., Banno, Y., Ono, Y., Yamada, S., Handa, M. (2023) Fatigue strength

of shot-peened welded joints of steel bridges, Welding in the World, Vol.67, pp.651-668, https://doi.org/10.1007/s40194-022-01400-7.
9. Meguid, S.A., Shagal, G., Stranart, J.C., Daly, J. (1999) Three-dimensional dynamic finite element analysis of shot-peening induced residual stresses, Finite Elements in Analysis and Design, Vol. 31, pp. 179-191, https://doi.org/10.1016/S0168-874X(98)00057-2.
10. Guagliano, M. (2001) Relating Almen intensity to residual stresses induced by shot peening: a numerical approach, Journal of Materials Processing Technology, Vol. 110, pp. 277-286, https://doi.org/10.1016/S0924-0136(00)00893-1.
11. Wang, X., Wang, Z., Wu, G., Gan, J., Yang, Y., Huang, H., He, J., Zhong, H. (2019) Combining the finite element method and response surface methodology for optimization of shot peening parameters, International Journal of Fatigue, Vol. 129 105231, https://doi.org/10.1016/j.ijfatigue.2019.105231.
12. Meo, M., Vignjevic, R. (2003) Finite element analysis of residual stress induced by shot peening process, Advances in Engineering Software, Vol. 34, pp. 569-575, https://doi.org/10.1016/S0965-9978(03)00063-2.
13. Ikushima, K., Shibahara, M., Akita, K., Suzuki, H., Morooka, S., Nishikawa, S., Furukawa, T. (2017) Numerical analysis of residual stress distribution on peening process, Weld World, Vol. 61, pp. 517-527, https://doi.org/10.1007/s40194-017-0430-4.
14. Badrinarayan, P.A., Natendra, P.S., Lingyun, P., Wei, H., Mark, J., James, A.F. (2013) A computation approach for fatigue life prediction in shot peened welded specimens, Welding World, Vol.57, pp.675-684, https://doi.org/10.1007/s40194-013-0065-z.
15. Nordin, E., Alfredsson, B. (2016) Measuring shot peening media velocity by indent size comparison, Journal of Materials Processing Technology, Vol. 235, pp.143-148, https://doi.org/10.1016/j.jmatprotec.2016.04.012.
16. Gariépy, A., Miao, H.Y., Lévesque, M. (2017) Simulation of the shot peening process with variable shot diameters and impacting velocities, Advanced in Engineering Software, Vol. 114, pp.121-133, https://doi.org/10.1016/j.advengsoft.2017.06.011.
17. Ogawa, K., Asano, T., Saito, A., Kawamura, K., Ogino, M., Aihara, H. (1994) Measurement and Analysis of Shot Velocity in Pneumatic Shot Peening, The Japan Society of Mechanical Engineers, Vol.60, No.571, pp.392-397, https://doi.org/10.1299/kikaic.60.1120. (In Japanese)
18. Nambu, K., Ito, K., Egami, N. (2010) Numerical Calculation of Particles Velocity under the Compressible Fluid in Fine Particle Bombardments, The Japan Society of Mechanical Engineers, Vol.76, No.772, pp.546-553, https://doi.org/10.1299/kikaic.76.3728. (In Japanese)
19. Ohta, T., Tsutsumi, S., Ma, N. (2021) Direct measurement of shot velocity and numerical analysis of residual stress from pneumatic shot peening, Surfaces and Interfaces, Vol.22, https://doi.org/10.1016/j.surfin.2020.100827.
20. Takai, Y., Kinoshita, K., Inoue, K., Ono, S., Yamada, S. (2022) Investigation of reproducibility of numerical analysis based on shot velocity measurement, Proceedings of Construction Steel, Vol. 30, pp.422-427. (In Japanese)
21. Takai, Y., Kinoshita, K. (2021) Analytical Investigation on Shot Peening for Steel Materials, Proceedings of Construction Steel, Vol. 29, pp.441-448. (In Japanese)
22. Clausen, R., Stangenberg, J. (2003) Device for the Determination of Impact Velocities in Shot Peening, Proceedings of the 8th International Conference on Shot Peening, Mishiwaka, IN, Electronics Inc., pp. 89-95, https://doi.org/10.1002/3527606580.ch12.

23. Kirk, D. (2007) Generation of air-blast shot velocity, The Shot Peener Magazine, Vol. 2, pp.24-30.
24. Zinn, W., Schulz, J., Kopp, R., Scholtes, B. (2002) The influence of the velocity of a peening medium on the Almen intensities and residual stress states of shot peened specimen, Proceedings of the 8th International Conference on Shot Peening, Mishiwaka, IN, Electronics Inc., pp. 161-166, https://doi.org/10.1002/3527606580.ch21.
25. Takahashi, T., Yamada, T., Ishikawa, T. (2009) Investigation of Plastic Strain Profile after Shot Peening by Finite Element Method, Journal of Japan for Society for Technology of Plasticity, Vol. 50, no. 577, pp. 114-118, https://doi.org/10.9773/sosei.50.114. (in Japanese)
26. Altair Radioss, https://2021.help.altair.com/2021/hwsolvers/rad/topics/getting_started/user_guide_overview_rad_c.htm.
27. Kitamura, Y. (2015) Study on Stress relaxation Behavior during Shot Peening, 2015th Gradual Thesis Summary of Osakahuritsu University, pp. B07-1-B07-4 (in Japanese)
28. Ernould, C., Schubnell, J., Farajian, M., Maciolek, A., Simunek, D., Leitner, M., Stoschka, M. (2019) Application of different simulation approaches to numerically optimize high-frequency mechanical impact (HFMI) post-treatment process, Welding in the World, Vol.63, pp.725-738, https://doi.org/10.1007/s40194-019-00701-8.
29. Schulze, V., Klemenz, M., Zimmermann, M. (2008) State of the Art in Shot Peening Simulation, International Scientific Committee for Shot Peening 10 Tokyo Japan.
30. Rahmaan. T., Noder, J., Abedini, A., Zhou, P., Butcher, C. (2020) Anisotropic plasticity characterization of 6000- and 7000- series aluminum sheet alloys at various strain rates, International Journal of Impact Engineering, Vol. 135, https://doi.org/10.1016/j.ijimpeng.2019.103390.
31. Yadav, S., Singhal, S., Jasra, Y., Saxena K, R. (2020) Determination of Johnson-Cook material model for weldment of mild steel, Material Today: Proceedings, Vol.28, pp.1801-180, https://doi.org/10.1016/j.matpr.2020.05.213.
32. Forni, D., Chiaia, B., Cadoni, E. (2016) Strain rate behavior in tension of S355 steel: Base for progressive collapse analysis, Engineering Structures, Vol.119, pp.164-173, https://doi.org/10.1016/j.engstruct.2016.04.013.
33. Banno, Y., Kinoshita, K., Ishikawa, T., Anami, K. (2020) Influence of grid blast on the fatigue strength improvement by peenng, The 10th International Conference on Bridge Maintenance, Safety and Management (IABMAS2020), pp.3165-3173, 2020.
34. Ahola, A., Lipiäinen, K., Riski, J., Koskimäki, M., Pyörret, J., Björk, T. (2023) Fatigue strength of shot-peened as-welded joints and post-weld treated and subsequently clean-blasted fillet weld joints, Welding in the World, Vol. 67, pp.1559-1574, https://doi.org/10.1007/s40194-023-01498-3.

Author contribution Conceptualization: Y. Takai, Y. Ono, Y. Banno; Methodology: K. Kinoshita, Y. Takai, Y. Ono, Y. Banno, K. Inoue; Validation: Y. Takai, Y. Ono, Y. Banno; Formal analysis and investigation: Y. Takai, Y. Ono, Y. Banno, K. Inoue; Resources: K. Kinoshita; Data Curation: Y. Takai, Y. Ono, Y. Banno, K. Inoue; Writing - original draft preparation: Y. Banno; Writing - review and editing: K. Kinoshita, Y. Ono; Visualization: Y. Takai, Y. Ono, Y. Banno; Supervision: K. Kinoshita; Project Administration: K. Kinoshita; Funding acquisition: K. Kinoshita.

Data availability Data generated during this study is available from the corresponding author on request.

Funding This research was supported by “The Japan Welding Society's Research Grant Program for Next-Generation Researchers in 2021” and by “The 11th Ueda Memorable Foundation”.

Declaration

Competing interests The authors declare no competing interests